Computer simulations of nanoindentation in Mg–Cu and Cu–Zr metallic glasses

Computer simulations of nanoindentation in Mg–Cu and Cu–Zr metallic glasses

A Păduraru[1], U G Andersen[2], A Thyssen[2], N P Bailey[3], K W Jacobsen[1] and J Schiøtz[2]

[1] Center for Atomic-scale Materials Design (CAMD), Department of Physics, Technical University of Denmark, DK-2800 Lyngby, Denmark
[2] Danish National Research Foundation's Center for Individual Nanoparticle Functionality (CINF), Department of Physics, Technical University of Denmark, DK-2800 Lyngby, Denmark
[3] Department of Mathematics and Physics (IMFUFA), DNRF Center 'Glass and Time', Roskilde University, PO Box 260, DK-4000 Roskilde, Denmark

E-mail: schiotz@fysik.dtu.dk

Abstract

The formation of shear bands during plastic deformation of $Cu_{0.50}Zr_{0.50}$ and $Mg_{0.85}Cu_{0.15}$ metallic glasses is studied using atomic-scale computer simulations. The atomic interactions are described using realistic many-body potentials within the effective medium theory, and are compared with similar simulations using a Lennard-Jones description of the material. The metallic glasses are deformed both in simple shear and in a simulated nanoindentation experiment. Plastic shear localizes into shear bands with a width of approximately 5 nm in CuZr and 8 nm in MgCu. In simple shear, the shear band formation is very clear, whereas only incipient shear bands are seen in nanoindentation. The shear band formation during nanoindentation is sensitive to the indentation velocity, indenter radius and the cooling rate during the formation of the metallic glass. For comparison, a similar nanoindentation simulation was made with a nanocrystalline sample, showing how the presence of a polycrystalline structure leads to a different and more spatially distributed deformation pattern, where dislocation avalanches play an important role.

(Some figures in this article are in colour only in the electronic version)

1. Introduction

Since the discovery of metallic glasses [1], there has been a great interest in understanding and improving their mechanical properties [2, 3]. The main obstacle for applications of bulk metallic glasses is their brittleness, due to intense localization of the plastic deformation into shear bands. This localization is presumably due to the lack of work hardening

in amorphous alloys. This difference between the macroscopic mechanical behavior of amorphous and crystalline alloys is caused by the fundamentally different atomic-scale deformation mechanisms of the two classes of materials. In crystalline alloys, plastic deformation is carried by dislocations, which multiply and eventually entangle in a deforming crystal, leading to work hardening [4]. In an amorphous alloy, dislocations are not possible due to the lack of a crystal structure, and deformation proceeds through localized deformation events [5–9]. Since these events do not lead to local strengthening, deformation may localize into shear bands.

For these reasons, much work has been done to study deformation and shear band formation in metallic glasses with atomic-scale simulation methods [9–18]. Most of this work has been done with Lennard-Jones (LJ) model systems, sometimes in two dimensions to make the system sizes larger for the same computational burden. While LJ systems can capture much of the essential physics of a deforming metallic glass, the description of the atomic interactions is too simple to give a realistic description of a *specific* metallic glass. For such a purpose, many-body potentials such as the embedded atom method [19] or the effective medium theory (EMT) [20, 21] must be used, at the price of a significant increase in the computational burden.

We have previously shown that computer simulations can capture the formation of shear bands in MgCu metallic glass, deformed under tension in plane strain [15]. In this paper, we study the formation of shear bands under nanoindentation of a CuZr glass and a MgCu glass. CuZr was recently discovered to be a binary bulk metallic glass [22, 23]. Since binary alloys are easier to model than alloys with more elements, this makes CuZr an attractive bulk metallic glass to study theoretically.

2. Creating virtual metallic glass samples

We perform quasi-two-dimensional molecular dynamics simulations on binary alloys in order to simulate nanoindentation. The materials are $Cu_{0.50}Zr_{0.50}$ and $Mg_{0.85}Cu_{0.15}$, described with EMT potentials [21] recently fitted to describe these materials [24, 25]. Samples of metallic glass were produced by cooling the systems at a constant pressure from 1400 K (well above the melting temperature) to the final temperature in steps of 25 K, with an average cooling rate of $0.54 \, K \, ps^{-1}$, following the procedure published previously [25]. In all cases periodic boundary conditions were used along all three axes during the cooling procedure, for the subsequent deformation simulations the periodicity along one axis was removed.

Samples with two sizes were made. Small samples containing 62 400 atoms were produced to be used for simple shear deformation. The sample dimensions were 52.9 nm × 12.2 nm × 1.6 nm for CuZr and 57.0 nm × 13.1 nm × 1.7 nm for MgCu. These samples were cooled to 50 K.

Much larger samples were needed for the nanoindentation simulations: samples were created with dimensions of 52.9 nm × 52.9 nm × 1.6 nm for CuZr and 57.2 nm × 57.2 nm × 1.7 nm for MgCu, both corresponding to 270 000 atoms. These samples were cooled to 116 K. Before nanoindentation, the samples were replicated in the *x* direction, giving, e.g. a CuZr sample size of 105.9 nm × 52.9 nm × 1.6 nm, with periodic boundary conditions along the *x* and *z* directions, and free boundaries in the *y* direction.

In order to compare with previously published results, we also created equivalent CuZr samples for nanoindentation simulations using the LJ potential. We used the same parameters as in the simulations by Shi and Falk [26]. There is no absolute distance and energy scales in a LJ simulation, we used that freedom to scale the parameters in order to get a system with properties close to the EMT description of CuZr. We used the LJ parameters $\varepsilon_{CuCu} = \varepsilon_{ZrZr} = 0.1 \, eV$; $\varepsilon_{CuZr} = 0.2 \, eV$; $\sigma_{CuCu} = 1.236 \, \text{Å}$; $\sigma_{ZrZr} = 2.352 \, \text{Å}$; $\sigma_{CuZr} = 2.0 \, \text{Å}$.
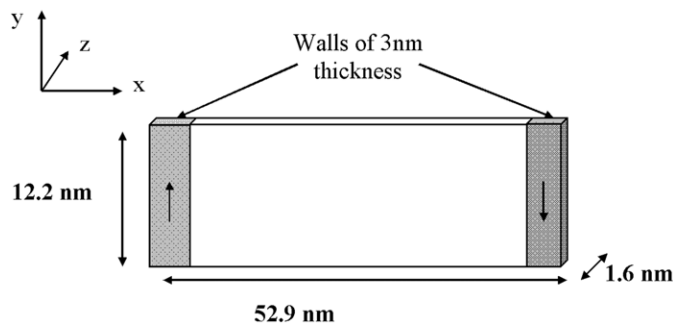
Figure 1. The setup used for simple shear deformations. The shear is applied by forcing the walls to move as indicated by the arrows. There are periodic boundary conditions in the *y* and *z* directions.

This gives a material with a glass-transition temperature of approximately 575 K, compared with 620 K for the EMT description of CuZr.

The LJ samples were created with dimensions of 89.6 nm × 44.8 × 1.4 nm, corresponding to 551120 atoms, which is very close to the amount in the replicated EMT samples. These samples were produced by equilibrating the systems for 25 000 timesteps at 1000 K, which is well above the melting temperature of this system. They were subsequently cooled to 108 K, corresponding to the same ratio of glass-transition temperature to indentation temperature as for the EMT simulations; the cooling rate was scaled similarly. As can be seen from the dimensions, these samples were not replicated, as the lower computational burden of the LJ potential made is relatively easy to cool the full sample.

3. Deformation in simple shear

We deformed the metallic glasses under simple shear, using a geometry illustrated in figure 1. The sample is divided into three parts, two outer 'walls' of 3 nm thickness, and a central part. In the central part, the dynamics of the atoms is left unperturbed, but in the two walls the center of mass motion is constrained, hence the two walls move with a constant relative speed. The atoms in the walls are not held rigid; they can still move with respect to each other, since only the mass-weighted sum of their velocities is held fixed. By causing one wall to move in the *y*-direction, a shear deformation with constant shear rate is applied to the system. The system has periodic boundary conditions in the *y* and *z* directions, but free boundaries in the *x* direction. The shear simulations are done at a temperature of 50 K.

During the deformation, velocity profiles (average atomic velocities as a function of *x*-coordinate) are calculated. Both velocity profiles and plots of the deformed system clearly show the formation of shear bands (see figure 2). Visual inspection indicates that the width of the shear bands is 5 nm for the CuZr glass, and almost 10 nm for the MgCu glass; the latter is consistent with the simulations of Bailey *et al* [15]. A better estimate can be obtained by fitting the velocity profiles to a Fermi function $1/(\exp(x/\alpha) + 1)$ or to the $\arctan(x/\alpha)$ function, the former gives a slightly better fit as the tails of the arctan function are too large. This gives a width parameter α of 1.51 nm for CuZr and 1.93 nm for CuMg, corresponding to shear band widths of 6 nm and 8 nm, respectively, as the majority of the variation of the Fermi function occurs in the interval from -2α to 2α. The fits to the arctan function give $\alpha = 1.23$ nm and 2.03 nm corresponding to shear band widths of 5 and 8 nm for CuZr and CuMg. In all cases the fits were done with four free parameters: the width, an amplitude and two translations.
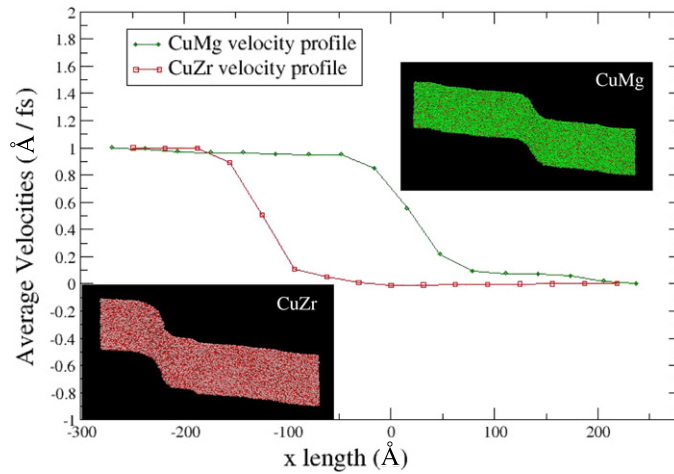
3

Figure 2. Shear deformation on CuZr and MgCu thin sample and the velocity profile with respect to the length. The width of the shear bands were found to be 5–6 nm for CuZr and 8 nm for MgCu.
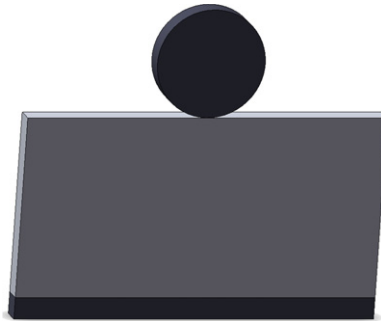

Figure 3. The geometry used during nanoindentation. The cylindrical indenter is modeled as a repulsive potential. There are periodic boundary conditions in the *x* and *y* directions (left-right and out of the plane of the paper). The upper surface is free, the lower surface is held fixed by fixing the positions of all atoms in a 0.8 nm thick layer.

For comparison, simulations were also done without the walls, but with full periodic boundary conditions in all three directions. The deformation was made by changing the shape of the computational box, i.e. changing one of the three vectors describing the periodicity of the system. The results were essentially the same.

4. Nanoindentation

To simulate nanoindentation, we perform molecular dynamics using Langevin dynamics [27] at a constant temperature of 116 K. During the simulation, an indenter is pushed into the sample at constant velocity. Since the samples are very thin in the *z* direction, the simulation is quasi-two dimensional, and we choose to use a cylindrical indenter (see figure 3). The indenter is modeled as a repulsive potential, as proposed by Shi and Falk [28]. The form of the repulsive potential is

$$E = c(r_{xy} - R)^{-6}, \tag{1}$$

where r_{xy} is the distance in the x–y plane from the center of the indenter to the atom and R the indenter radius. The strength parameter $c = 2.0\,\text{eV}\,\text{Å}^6$. The indenter is lowered into the substrate under displacement control recording at each step the load and the total displacement. During indentation, the lower edge of the system is held fixed by fixing the positions of the atoms in the bottom 0.8 nm of the system. The thickness of the system is kept constant during the indentation (plane strain).

To visualize the plastic flow and the localization of the shear bands we use the $D_{\min}^2$ method introduced by Falk and Langer [11]. $D_{\min}^2$ quantifies the local deviation from affine deformation during the interval of time between a pair of configurations.

4.1. Formation of shear bands under the nanoindenter

A nanoindentation simulation is performed on the CuZr sample as described above. The cylindrical indenter with a radius of 30 nm is indented into the sample with a velocity of $7\,\text{m}\,\text{s}^{-1}$, as illustrated in figure 3. As the shear is inhomogeneous, it is not possible to rigorously define an equivalent shear rate, but it corresponds roughly to a shear rate of the order of $10^8\,\text{s}^{-1}$ (a homogeneous shear rate of $10^8\,\text{s}^{-1}$ would correspond to the ends of the sample moving with a relative velocity of $10\,\text{m}\,\text{s}^{-1}$).

During nanoindentation, the net force on the indenter is recorded as a function of indentation depth, see figure 4. The curve is not smooth, but contains small serrations, presumably reflecting individual events during deformation. It would be tempting to interpret this as the formation of individual shear bands, but that interpretation is not supported by direct visualization of the shear band formation. As seen in figure 4, the shear bands are not formed at once, but grow gradually during the nanoindentation. Just like in the simulations of Shi and Falk [16], the curved shape of the emerging shear bands corresponds to the expected directions of the maximally resolved shear stress, as predicted by slip line theory [29].

The shear bands are less clearly formed than in the simulations of Shi and Falk [26] but very similar to those of Jiang *et al* [30]; this will be discussed further in section 4.3.

4.2. Influences on the shear band formation

In this section we study how the shear band formation is influenced by varying the parameters of the nanoindentation, corresponding to varying physical parameters during a nanoindentation experiment. We vary the indenter velocity, its radius, the cooling rate during glass formation and the composition of the glass. All modifications are relative to a 'standard simulation' of a CuZr metallic glass produced at a cooling rate of $0.44\,\text{K}\,\text{ps}^{-1}$, indented with a cylindrical indenter of radius 30 nm and indentation velocity $7\,\text{m}\,\text{s}^{-1}$.

Figure 5 shows how the shear band formation is influenced by the indentation velocity. A simulation with an indentation velocity of $30\,\text{m}\,\text{s}^{-1}$ is compared with the reference simulation. The shear band formation is less obvious in the fast indentation. A clear indentation rate dependence of the load–displacement curve is also seen; the loading force—and thus the stress in the material—is significantly higher during the fast simulation, but no qualitative differences are seen. It can be speculated that even lower indentation rates will lead to formation of fewer and larger shear bands, and possibly lead to macroscopic failure through a few very large shear bands [31].

Despite the indenter diameter being an order of magnitude larger than the width of the shear band, a difference is also seen when the indenter radius is varied. This is illustrated in figure 6, where the effect of reducing the indenter radius by 33% is studied. As seen, fewer
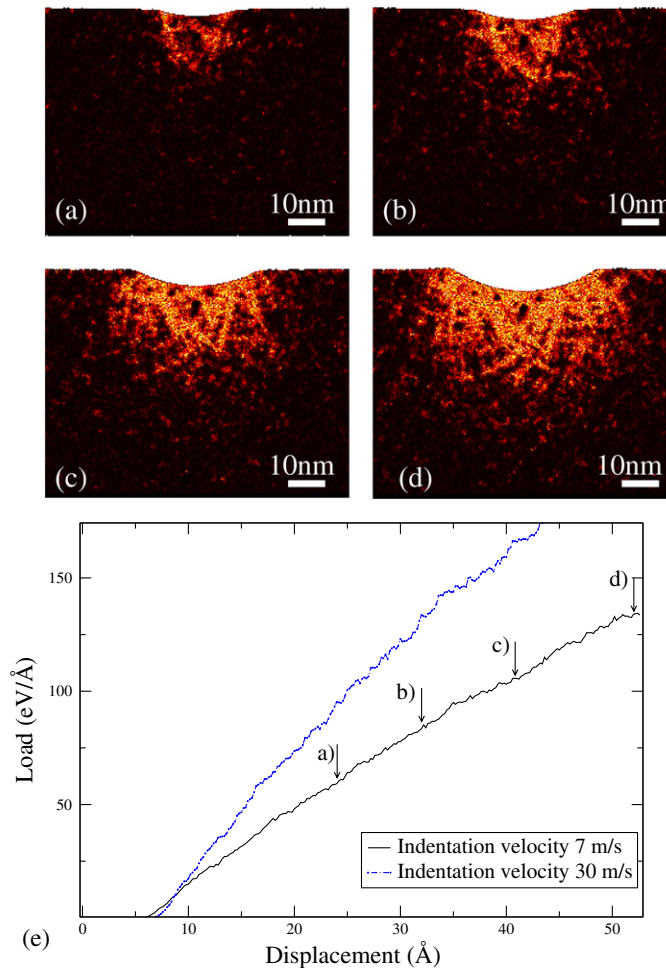
Figure 4. Development of shear bands during nanoindentation on a Cu–Zr thin sample: (*a*)–(*d*) visualization of strain localization at 24, 32, 42 and 52 Å depth of the indenter, the indentation velocity was $7\,\mathrm{m\,s^{-1}}$; (*e*) the lower curve is the corresponding load–displacement curve, the displacements corresponding to the four panels are shown with arrows. It is seen that the shear bands form gradually: there is no correspondence between events on the indentation force curve and formation of shear bands. The upper curve is a similar indentation when the indentation velocity is increased to $30\,\mathrm{m\,s^{-1}}$.

shear bands are formed, when we have chosen to compare situations with the same indentation depth. It is likely that this difference is at least partly caused by less material being displaced by the smaller indenter.

The effect of changing the cooling rate during the glass formation is investigated in figure 7, where identical nanoindentation simulations are performed on two samples produced with cooling rates of $2.2\,\mathrm{K\,ps^{-1}}$ and $0.44\,\mathrm{K\,ps^{-1}}$. In this case the difference is less pronounced, but the shear band appears more distinct in the slowly cooled sample. This is consistent with results by Shi and Falk [28] showing a stronger tendency for shear localization for slowly annealed systems. The cause is most likely that stronger annealing causes a larger fraction of the atoms locally to be in energetically favorable structures. As it costs energy to break these structures,
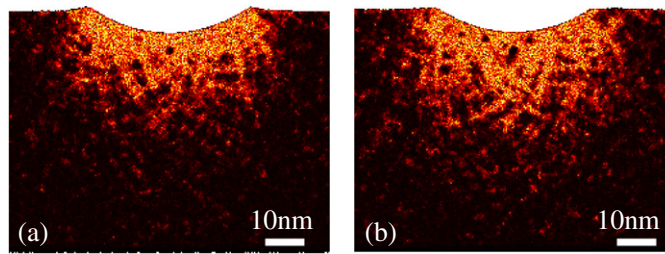
Figure 5. Influence of varying the indentation velocity on shear band formation and on load–displacement curves. The indentation velocities are $30 \, m \, s^{-1}$ (panel a) and $7 \, m \, s^{-1}$ (panel b). The shear bands are less developed during the fast nanoindentation. The corresponding load–displacement curves are shown in figure 4(*e*).
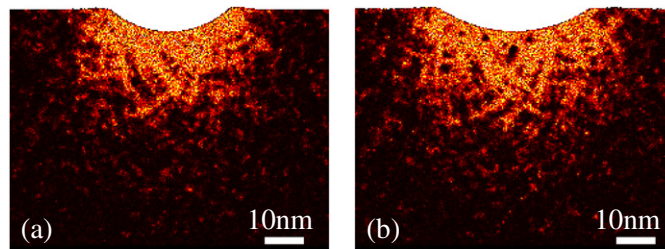

Figure 6. Influence of varying the indenter radius. The radii are 20 nm (*a*) and 30 nm (*b*); more shear band formation is observed under the larger indenter.
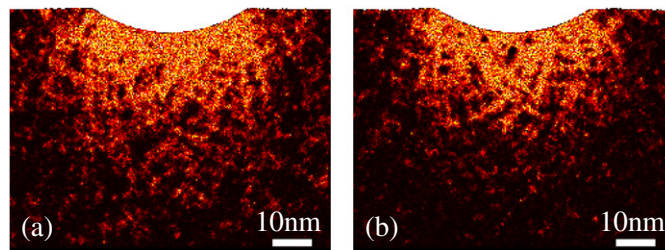

Figure 7. Influence of varying the cooling rate during glass formation. Samples created with cooling rates of $2.2 \, K \, ps^{-1}$ (*a*) and $0.44 \, K \, ps^{-1}$ (*b*) were subjected to otherwise identical nanoindentation simulations. The shear localization appears stronger in the more slowly cooled sample.

they will strengthen the material, and local softening occurs when deformation breaks them up. This effect is weakened in insufficiently annealed samples. In the two-dimensional glass of Shi and Falk, these local structures have quasi-crystalline order [28]; we cannot, however, say anything about the local order in the more complicated case of a three-dimensional glass.

Finally, we investigated the consequences of replacing the CuZr glass with a MgCu glass (figure 8). Shear localization is far more pronounced in the CuZr sample. This is consistent with our previous findings that shear bands are approximately twice as wide in the MgCu glass (see also figure 2).
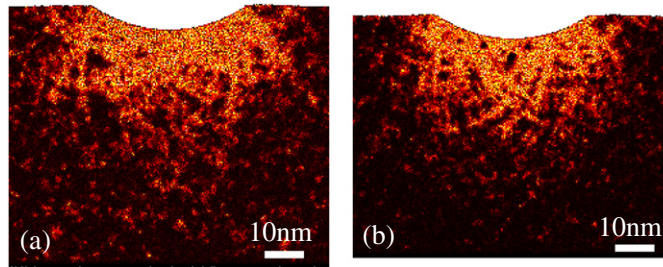
7

Figure 8. Comparison of MgCu (*a*) and CuZr (*b*) metallic glass under otherwise identical nanoindentation conditions. The latter shows the strongest shear localization.
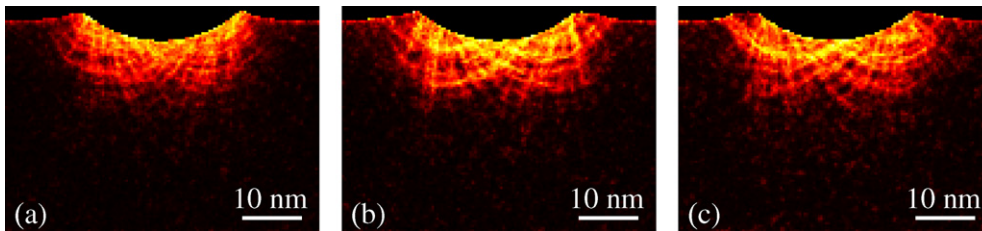

Figure 9. CuZr modelled with a LJ potential. The middle image (*b*) is simulated with the same parameters as the reference EMT simulation. Comparing (*a*) and (*b*) shows the effect of varying the indentation rate from $30\,\mathrm{m\,s^{-1}}$ in (*a*) to $7\,\mathrm{m\,s^{-1}}$ in (*b*), the strain localization is seen to be stronger when indenting slowly. Comparing (*b*) and (*c*) shows that no detectable change is seen when changing the cooling rate from 0.41 to $2.0\,\mathrm{K\,ps^{-1}}$.

4.3. Comparison with LJ simulations

The simulations reported in the previous section differ qualitatively from previously published results, e.g. by Shi and Falk [26]. The most prominent difference is that the shear bands are far more localized in the simulations by Shi and Falk. The main difference between the simulations is the description of the interatomic interactions (EMT versus LJ), the dimensionality of the systems and the indentation rates. Most previously published LJ-based simulations are two dimensional to reduce the computational burden. Our simulations have a finite albeit small thickness, hence although the overall geometry is quasi-two dimensional the atoms are free to move in the third dimension. This finite thickness, in combination with the more complex EMT potential, makes the computational burden larger and the simulations are therefore by necessity performed with a higher indentation rate.

There are thus three major differences between these simulations and the simulations by Shi and Falk: the dimensionality, the potential and the indentation speed, and it is not surprising that the results are somewhat different. In order to investigate the relative importance of these differences, simulations were performed with LJ systems, both in a geometry similar to the EMT simulations, and for two-dimensional systems.

Figure 9 shows the results for the 3D LJ simulations. We see that the systems are not qualitatively different from the EMT systems, although a clear tendency for a somewhat stronger shear localization is seen. Shear localization is reduced with the indentation rate, this is the same trend as observed for the EMT systems. The effect of varying the cooling rate is undetectable for the LJ systems, at least for the cooling rates studied here.
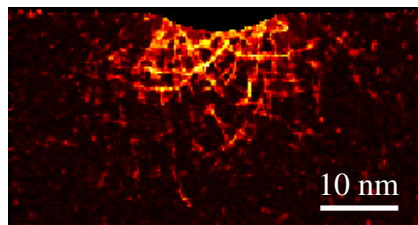
Figure 10. The shear bands are much more pronounced in a 2D simulation (using the LJ potential). The simulation shown is with an indentation rate of $7\,\mathrm{m\,s^{-1}}$ and a cooling rate of $0.41\,\mathrm{K\,ps^{-1}}$. Changing the indentation rate to $0.7\,\mathrm{m\,s^{-1}}$ does not change the pattern significantly (not shown).

Two two-dimensional simulations were performed to investigate the effect of dimensionality, they are shown in figure 10. Clearly, the shear localizes far more strongly in two dimensions, leading to the conclusion that the different dimensionality is the major difference between the simulations published here and previous results.

5. Nanoindentation of nanocrystalline samples

For comparison, we subjected a nanocrystalline sample to indentation in a similar manner. Nanoindentation of nanocrystalline samples has previously been studied by Van Swygenhoven *et al* [32, 33] with a particular focus on the onset of plastic deformation under a spherical indenter. In this work we have chosen to mimic the indentation parameters used for the metallic glass, hence the nanocrystalline sample is quasi-two dimensional with $\langle 1\,1\,0 \rangle$-directions along the thin direction (the z direction). This orientation is chosen to maximize the number of possible slip systems in the crystal, which is nevertheless still significantly lower than in a full three-dimensional simulation [34]. The material for this simulation is copper, described with the EMT potential [21].

The nanocrystalline sample was made by a random Voronoi construction. Random grain centers were chosen, and the part of space closer to a given grain center than to any other grain center was filled with a randomly rotated crystal, as published previously [35].

The sample has the same dimensions as the CuZr metallic glass sample, and similarly to the glassy sample, it is made by repeating a system with half the size in the x direction. The average grain diameter is 15 nm. The annealing is, however, only done from a temperature of 464 K ($kT = 0.04$ eV), staying well below the melting point to preserve the nanocrystalline structure. The indentation is done to a depth of around 5 nm, comparable to the simulations with metallic glass. After the simulation, the local atomic structure is analyzed with the common neighbor analysis [36], identifying atoms which are locally coordinated as face-centered cubic (grain interiors), hexagonal closed-packed (stacking faults and twin boundaries) or otherwise (grain boundaries and dislocation cores).

Figure 11 shows the deformation during this nanoindentation and figure 12 the corresponding load–displacement curves. A number of noteworthy features are marked by letters in figure 11(*b*).

Right below the indenter (marked 'A'), the plastic deformation is severe, and several grain boundaries have disappeared. These are low-angle grain boundaries, which can be regarded as dense arrays of dislocations. The high stress below the indenter causes these to move. Many stacking faults are seen; they are caused by the high stress levels, making the energy of the stacking fault irrelevant compared with the elastic energy. Another example of a low-angle grain boundary disappearing as a result of dislocation migration is marked 'B'.
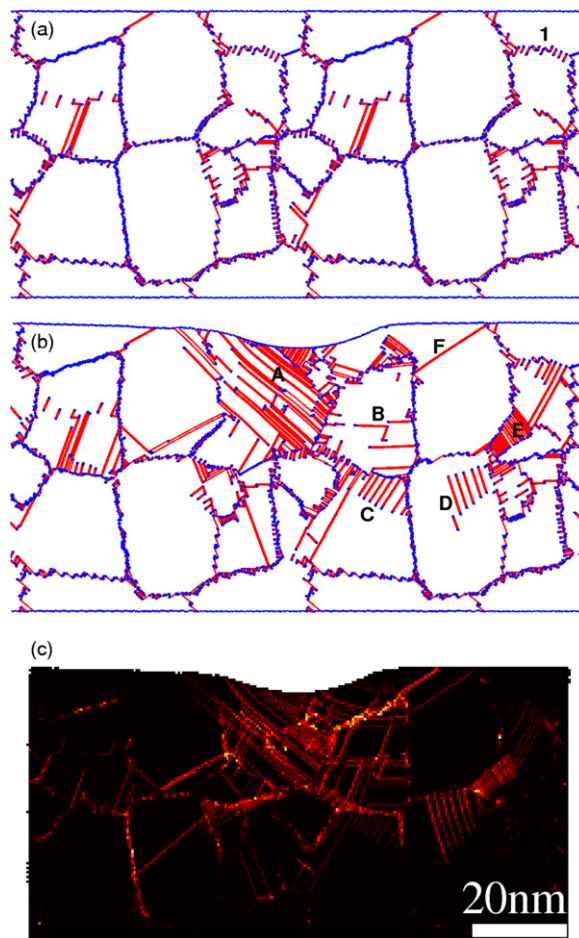
Figure 11. Nanoindentation of nanocrystalline copper. (*a*) The initial configuration before indentation. Atoms in the grain interiors are not shown; atoms at stacking faults and twin boundaries are colored red (light grey in print); atoms in grain boundaries, dislocation cores and at surfaces are blue (dark grey in print). Both high-angle and low-angle grain boundaries are seen, the former are shown as blue (dark grey in print) walls, the latter are seen to be made of individual dislocations, for example the one marked '1'. A few stacking faults created by dislocation activity during annealing are also seen. (*b*) After nanoindentation, significant plastic deformation has occurred, in particular just under the indenter, where numerous stacking faults and deformation twins have appeared. The letters A–F mark features discussed in the text. (*c*) A deformation map shows that the majority of the deformation occurs inside the grains and is caused by dislocation activity, although some grain boundary sliding is also seen.

A few grain boundaries 'reconstruct' under the applied stress by emitting an array of partial dislocations (for example at 'C'). Presumably a lower grain boundary energy can be obtained and some of the applied stress relieved by the motion of the dislocation wall, at the expense of creating some stacking faults. A similar phenomenon is seen at 'D', where a wall of dissociated dislocations has been emitted by the grain boundary, and an extreme case at 'E', where a grain boundary has split into two separated by a region of (slightly faulted) HCP crystal. Similar reconstructions of grain boundaries under stress have previously been seen in computer simulations [37]. At 'F' a stacking fault has been removed by the motion of a
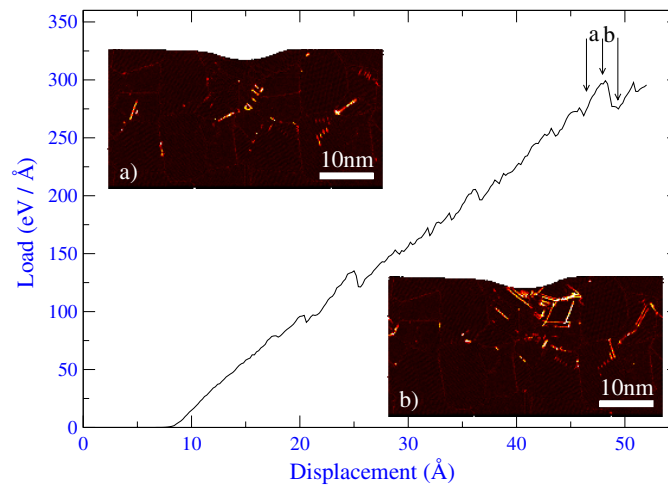
Figure 12. Load–displacement curve during nanoindentation of the crystal. The insets marked a and b show the deformation occurring in the two intervals between the arrows.

partial dislocation, and a new one has been created nearby by an independent event, creating the illusion that a stacking fault has moved.

The events discussed above can also be found in the displacement map in figure 11(*c*). The figure shows a striking difference between the deformation distributions in the glass and in the nanocrystalline sample: in the crystalline sample the spatial distribution of the deformation is much more uneven, as it is controlled by the polycrystalline structure. Deformation can only occur at grain boundaries, or where dislocations are available, typically from grain boundary sources.

The load–displacement curve in figure 12 shows significantly larger serrations than for the glassy samples. This is caused by avalanches of dislocation activity [38]. The insets show how the deformation occurs just before and during one of the serrations. It is clearly seen that the serration does not correspond to a single dislocation event but rather to an avalanche of events.

6. Summary and conclusion

We have investigated shear band formation during homogeneous shear and during nanoindentation in CuZr- and MgCu-based metallic glasses, using realistic interatomic potentials within the EMT. In homogeneous shear, shear bands of 5 and 8 nm thickness form in the CuZr- and MgCu-based glasses, respectively. In nanoindentation, we see a clear signature of shear band formation under the indenter, although the shear bands are not as well developed as in two-dimensional LJ simulations. The shear bands form gradually during indentation. Shear band formation is stronger if the indentation velocity is low, if the indenter is large and if the sample was cooled slowly. In addition, shear bands were clearer in CuZr than in MgCu under otherwise identical conditions, probably due to the natural width of the shear bands in MgCu being larger.

Simulations of nanoindentation in nanocrystalline copper under otherwise identical conditions show a significantly different deformation mechanism, where individual dislocations strongly influence the deformation pattern.

11

Acknowledgments

References

[1] Klement W, Willens R H and Duwez P 1960 *Nature* **187** 869–70
[2] Greer A L 1995 *Science* **267** 1947–53
[3] Inoue A 2000 *Acta Mater.* **48** 279–306
[4] Hirth J P and Lothe J 1992 *Theory of Dislocations* 2nd edn (Malabar, FL: Krieger)
[5] Argon A S 1979 *Acta Metall.* **27** 47–58
[6] Khonik V A, Kosilov A T, Mikhailov V A and Sviridov V V 1998 *Acta Mater.* **46** 3399–408
[7] Ibenskas A, Lekka C E and Evangelakis G A 2007 *Physica* E **37** 189–193
[8] Lekka C E, Ibenskas A, Yavari A R and Evangelakis G A 2007 *Appl. Phys. Lett.* **91** 214103
[9] Bailey N P, Schiøtz J, Lemaître A and Jacobsen K W 2007 *Phys. Rev. Lett.* **98** 095501
[10] Deng D, Argon A S and Yip S 1989 *Philos. Trans. R. Soc. Lond. Ser.* A **329** 613
[11] Falk M L and Langer J S 1998 *Phys. Rev.* E **57** 7192–205
[12] Varnik F, Bocquet L, Barrat J L and Berthier L 2003 *Phys. Rev. Lett.* **90** 095702
[13] Bailey N P, Schiøtz J and Jacobsen K W 2004 *Mater. Sci. Eng.* A **387–389** 996–1000
[14] Shi Y F and Falk M L 2005 *Phys. Rev. Lett.* **95** 095502
[15] Bailey N P, Schiøtz J and Jacobsen K W 2006 *Phys. Rev.* B **73** 064108
[16] Shi Y F and Falk M L 2007 *Acta Mater.* **55** 4317–24
[17] Slufarska I 2006 *Mater. Today* **9** 42–50
[18] Mendelev M I, Ott R T, Heggen M, Feuerbacher M, Kramer M J and Sordelet D J 2008 *J. Appl. Phys.* **104** 123532
[19] Daw M S and Baskes M I 1984 *Phys. Rev.* B **29** 6443–53
[20] Jacobsen K W, Nørskov J K and Puska M J 1987 *Phys. Rev.* B **35** 7423–42
[21] Jacobsen K, Stoltze P and Nørskov J 1996 *Surf. Sci.* **366** 394–402
[22] Xu D H, Lohwongwatana B, Duan G, Johnson W L and Garland C 2004 *Acta Mater.* **52** 2621–4
[23] Ray R, Giessen B C and Grant N J 1968 *Scr. Metall.* **2** 357–359
[24] Bailey N P, Schiøtz J and Jacobsen K W 2004 *Phys. Rev.* B **69** 144205
[25] Paduraru A, Kenoufi A, Bailey N P and Schiøtz J 2007 *Adv. Eng. Mater.* **9** 505
[26] Shi Y F and Falk M L 2007 *Thin Solid Films* **515** 3179–82
[27] Allen M P and Tildesley D J 1987 *Computer Simulation of Liquids* (Oxford: Clarendon)
[28] Shi Y and Falk M L 2005 *Appl. Phys. Lett.* **86** 011914
[29] Hill R 1950 *The Mathematical Theory of Plasticity* (Oxford: Clarendon)
[30] Jiang S Y, Jiang M Q, Dai L H and Yao Y G 2008 *Nanoscale Res. Lett.* **3** 524–9
[31] Schuh C A and Nieh T G 2003 *Acta Mater.* **51** 87–99
[32] Van Swygenhoven H, Derlet P M and Hasnaoui A 2003 *Adv. Eng. Mater.* **5** 345–50
[33] Feichtinger D, Derlet P M and Van Swygenhoven H 2003 *Phys. Rev.* B **67** 024113
[34] Yamakov V, Wolf D, Salazar M, Phillpot S R and Gleiter H 2001 *Acta Mater.* **49** 2713–22
[35] Schiøtz J, Vegge T, Di Tolla F D and Jacobsen K W 1999 *Phys. Rev.* B **60** 11971–83
[36] Faken D and Jónsson H 1994 *Comput. Mater. Sci.* **2** 279–86
[37] Schiøtz J, Rasmussen T, Jacobsen K W and Nielsen O H 1996 *Phil. Mag. Lett.* **74** 339–44
[38] Csikor F F, Motz C, Weygand D, Zaiser M and Zapperi S 2007 *Science* **318** 251–4